CHEMISTRY OF MATERIALS
Article

Chem. Mater. **2009,** *21,* 3865–3870 3865
DOI:10.1021/cm9015386

Nanoporous Silver with Controllable Optical Properties Formed by Chemical Dealloying in Supercritical CO_2

Rachel Morrish and Anthony J. Muscat*

Department of Chemical and Environmental Engineering University of Arizona, Tucson, Arizona 85721

Received June 4, 2009. Revised Manuscript Received July 1, 2009

Nanoporous Ag was formed by selectively etching Cu from multiphase AgCu alloys using the oxidant hydrogen peroxide and the metal chelator hexafluoroacetylacetone (hfacH, 14 mM) dissolved in supercritical CO_2 (60 °C and 16 MPa). The Ag films were characterized using X-ray photoelectron spectroscopy (XPS), field emission scanning electron microscopy (FESEM), energy-dispersive X-ray spectroscopy (EDS), X-ray diffraction (XRD), and ultraviolet−visible absorption spectroscopy. Sequential oxidation and chelation produced 50−100 nm Ag ligaments that exhibited an asymmetric localized surface plasmon resonance (LSPR) peak in the green range (500−570 nm). Simultaneous oxidation and chelation produced 100−200 nm faceted Ag particles that exhibited a broader, symmetric LSPR peak centered in the red range (600−700 nm). Dealloying of phase domains containing Cu concentrations as low as 24 at % was possible. These results demonstrate a means for large-scale and low environmental footprint preparation of nanoporous metals with controllable optical properties.

Introduction

When alloyed together or with other metals, copper, silver, and gold form a wide array of predominantly nonstoichiometric compounds. Using these noble intermetallics as starting materials offers the possibility of introducing composition dependent structural features into porous films with unique properties. Submicrometer porous noble metals have been used in applications ranging from optical components,[1−6] catalysts,[7−11] and chemical sensors[12−15] to specialty materials.[16−18] One established technique to generate porosity is by dealloying, where one metal is selectively etched from an alloy creating a random porous structure composed primarily of the inert metal. The most common approach for selective etching is to immerse an alloy in a concentrated acid solution, which preferentially ionizes and dissolves the less noble metal. Because the pores evolve during metal dissolution, their morphology can be controlled by varying reaction conditions.[19−21] This yields pore sizes ranging from a few nanometers up to a micrometer.[22,23] An electric potential can be applied to hasten the process. Reported conditions for void formation during conventional dealloying include a substantial difference in the standard potential between the constituent elements ($\Delta\phi > 0.1$ V), fast surface diffusion of the inert metal, and a minimum starting composition of the selectively removed species, defined as the parting limit.[24] Many studies have been published characterizing and modeling the dealloying process in polar liquid solutions.[24−30] The

*Corresponding author. E-mail: muscat@erc.arizona.edu.

(1) Sun, Y.; Xia, Y. *J. Am. Chem. Soc.* **2004**, *126*, 3892.
(2) Maaroof, A. I.; Cortie, M. B.; Smith, G. B. *J. Opt. A* **2005**, *7*, 303.
(3) Yu, F.; Ahl, S.; Caminade, A. M.; Majoral, J. P.; Knoll, W.; Erlebacher, J. *Anal. Chem.* **2006**, *78*, 7346.
(4) Dixon, M. C.; Daniel, T. A.; Hieda, M.; Smilgies, D. M.; Chan, M. H. W.; Allara, D. L. *Langmuir* **2007**, *23*, 2414.
(5) Biener, J.; Nyce, G. W.; Hodge, A. M.; Biener, M. M.; Hamza, A. V.; Maier, S. A. *Adv. Mater.* **2008**, *20*, 1211.
(6) Ahl, S.; Cameron, P. J.; Liu, J.; Knoll, W.; Erlebacher, J.; Yu, F. *Plasmonics* **2008**, *3*, 13.
(7) Smith, A. J.; Tran, T.; Wainwright, M. S. *J. Appl. Electrochem.* **1999**, *29*, 1085.
(8) Koh, S.; Strasser, P. *J. Am. Chem. Soc.* **2005**, *129*, 12624.
(9) Xu, C.; Xu, X.; Su, J.; Ding, Y. *J. Cat.* **2007**, *252*, 243.
(10) Zeis, R.; Lei, T.; Sieradzki, K.; Snyder, J.; Erlebacher, J. *J. Cat.* **2008**, *253*, 132.
(11) Mani, P.; Srivastava, R.; Strasser, P. *J. Phys. Chem. C* **2008**, *112*, 2770.
(12) Park, S.; Chung, T. D.; Kim, H. C. *Anal. Chem.* **2003**, *75*, 3046.
(13) Mortari, A.; Maaroof, A.; Martin, D.; Cortie, M. B. *Sens. Actuators, B* **2007**, *123*, 262.
(14) Chapman, P. J.; Long, Z.; Datskos, P. G.; Archibald, R.; Sepaniak, M. J. *Anal. Chem.* **2007**, *79*, 7062.
(15) Li, Y.; Song, Y.; Yang, C.; Xia, X. *Electrochem. Commun.* **2007**, *9*, 981.
(16) Hieda, M.; Garcia, R.; Dixon, M.; Daniel, T.; Allara, D.; Chan, M. H. W. *Appl. Phys. Lett.* **2004**, *84*, 628.
(17) Weissmüller, J.; Viswanath, R. N.; Kramer, D.; Zimmer, P.; Würschum, R.; Gleiter, H. *Science* **2004**, *300*, 312.
(18) Biener, J.; Hodge, A. M.; Hamza, A. V.; Hsiung, L. M.; Satcher, J. H. *J. Appl. Phys.* **2005**, *97*, 024301.
(19) Erlebacher, J.; Aziz, M. J.; Karma, A.; Dimitrov, N.; Sieradzki, K. *Nature* **2001**, *410*, 450.
(20) Dursun, A.; Pugh, D. V.; Corcoran, S. G. *J. Electrochem. Soc.* **2003**, *150*, B355.
(21) Qian, L. H.; Chen, M. W. *Appl. Phys. Lett.* **2007**, *91*, 083105.
(22) Pugh, D. V.; Dursun, A.; Corcoran, S. G. *J. Mater. Res.* **2003**, *18*, 216.
(23) Li, R.; Sieradzki, K. *Phy. Rev. Lett.* **1992**, *68*, 1168.
(24) Erlebacher, J. *J. Electrochem. Soc.* **2004**, *151*, C614.
(25) Sieradzki, K.; Corderman, R. R.; Shukla, K. *Philos. Mag.* **1989**, *59*, 713.
(26) Newman, R. C.; Corcoran, S. G.; Erlebacher, J.; Aziz, M. J.; Sieradzki, K. *Mater. Res. Soc. Bull.* **1999**, *24*, 23.
(27) Martin, H.; Carro, P.; Creus, A. H.; Morales, J.; Fernandez, G.; Esparza, P.; Gonzalez, S.; Salvarezza, R. C.; Arvia, A. J. *J. Phys. Chem. B* **2000**, *104*, 8229.
(28) Dimitrov, N.; Mann, J. A.; Vukmirovic, M.; Sieradzki, K. *J. Electrochem. Soc.* **2000**, *147*, 3283.
(29) Schofield, E. *Trans. Inst. Met. Finishing* **2005**, *83*, 35.
(30) Lu, H.; Li, Y.; Wang, F. *Scr. Mater.* **2007**, *56*, 165.

© 2009 American Chemical Society
Published on Web 07/20/2009

combined effect of surface tension, wetting, solubility, and mass transport on pore structure is difficult to unravel.

An alternative approach to fabricate a porous material and exert control over its structure and properties is to use a supercritical fluid solvent. Supercritical CO_2 ($scCO_2$) is an extremely good solvent for small molecules and is used in the food and pharmaceutical industries to extract and isolate medicinals, pigments, flavors, fragrances, and essential oils from plant and animal materials without organic solvents. The density of $scCO_2$ is similar to that of a liquid, providing a high flux of molecules to a surface in contact with the fluid; however, the mass transfer resistance is low, close to that of a gas, because the diffusivity is 1−2 orders of magnitude higher than in a liquid.[31] A near-zero surface tension and a low viscosity similar to gases allow supercritical fluids to penetrate porous media. Studying dealloying in a nonpolar and electrically neutral solution may help reveal how formation of the nanoporous layer relies on fluid properties and surface chemistry, leading to a better understanding of fundamental dealloying mechanisms. Enlisting $scCO_2$ as a solvent for dealloying could mitigate the limitations imposed by aqueous solutions and avoid the use of strong acids. The low toxicity, ease of separation, and potential for recycle confer a favorable environmental performance. The synergistic combination of density, diffusivity, surface tension, and viscosity, as well as tuning using pressure, temperature, and cosolvents, endow supercritical CO_2 with exceptional capabilities for large-scale, sustainable manufacturing of nanomaterials.[31,32]

This work extends supercritical fluid etching of a single component metal to a multicomponent system and demonstrates dealloying of multiphase AgCu. Previous studies showed that by either sequential or simultaneous oxidation and chelation, blanket copper metal films and islands were etched in $scCO_2$.[33−37] The heterogeneous reaction of positively charged Cu atoms with chelators produced complexes that were soluble in the nonpolar, neutral fluid. Silver is inherently more resistant to oxidation than Cu and under most conditions, a AgCu alloy will form an oxide scale consisting of CuO and metallic Ag.[38] Starting with an intermetallic bulk AgCu compound, we prepared nanoporous Ag (npAg) by selective oxidation of Cu metal to Cu^{2+} and chemical dealloying using the chelator hexafluoroacetylacetone (hfacH) dissolved in $scCO_2$; the Ag was not etched but diffused on the surface forming the final porous structure. High-surface-area Ag is a particularly desirable material because of its applications in surface enhanced Raman spectroscopy (SERS),[39] cathodic reduction catalysis,[40] and as an antibiotic agent.[41] Nanoporous silver has previously been formed by dealloying AgAl in NaOH[40] as well as AgZn in both H_2SO_4[42] and a ZnCl ionic liquid mixture.[43] Although alloying and dealloying mechanisms have been observed by scanning tunneling microscopy (STM) during growth of Ag on Cu surfaces,[44] there are currently no published reports examining dealloying of the multiphase AgCu system in either a liquid or a supercritical fluid. Our results show that the mechanism of pore formation in $scCO_2$ dealloying bears similarities to conventional liquid phase processes, but that selective removal is possible over a wider range of alloy compositions compared to other noble metal systems. By varying the processing conditions, we achieved two distinct surface morphologies, each of which exhibited a characteristic localized surface plasmon resonance signature at optical wavelengths. This technique is demonstrated with the binary AgCu system, but should be generally applicable to any alloy where one metal can be preferentially oxidized.

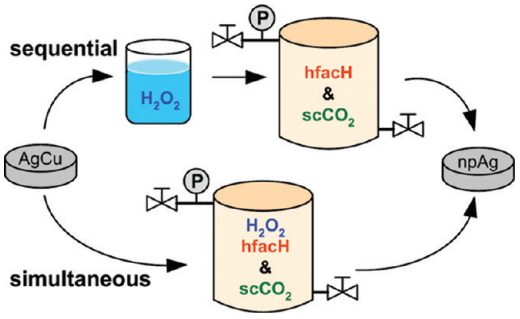

Figure 1. Schematic of the experimental methods showing sequential and simultaneous oxidation and dealloying of AgCu disks using H_2O_2 and hfacH dissolved in $scCO_2$.

Experimental Section

A 12.5 mm diameter AgCu alloy rod cast at its eutectic composition of 39.9 at % Cu was purchased from Goodfellow Cambridge Limited. The alloy was composed of Cu-rich lamella dispersed in a Ag-rich phase. Small, ~1 mm thick disks were cut from the rod and used for experimentation. As depicted in Figure 1, alloy samples were oxidized and etched using either sequential or simultaneous processes. In the sequential process, a disk was first immersed in liquid H_2O_2 to oxidize the surface and subsequently etched with hfacH dissolved in $scCO_2$. In the simultaneous process, a disk was oxidized and etched in situ by exposing to a mixture of H_2O_2 and hfacH dissolved in $scCO_2$.

For sequential dealloying, AgCu samples were oxidized at room temperature in 30% liquid H_2O_2 (General Chemical) for

(31) Johnston, K. P.; Shah, P. S. *Science* **2004**, *303*, 482.
(32) Cooper, A. I. *Adv. Mater.* **2003**, *15*, 1049.
(33) Murzin, A. A.; Babain, V. A.; Shadrin, A. Y.; Kamachev, V. A.; Strelkov, S. A.; Kiseleva, R. N.; Shafikov, D. N.; Podoinitsyn, S. V.; Kovalev, D. N. *Radiochemistry* **2003**, *45*, 131.
(34) Bessel, C. A.; Denison, G. M.; DeSimone, J. M.; DeYoung, J.; Gross, S.; Schauer, C. K.; Visintin, P. M. *J. Am. Chem. Soc.* **2003**, *125*, 4980.
(35) Xie, B.; Finstad, C. C.; Muscat, A. J. *Chem. Mater.* **2005**, *17*, 1753.
(36) Wang, J. S.; Wai, C. M. *Ind. Eng. Chem. Res.* **2005**, *44*, 922.
(37) Durando, M.; Morrish, R.; Muscat, A. J. *J. Am. Chem. Soc.* **2008**, *130*, 16659.
(38) Kubaschewski, O.; Hopkins, B. E. *Oxidation of Metals and Alloys*; Butterworth and Co.: London, 1962.
(39) Schwartzberg, A. M.; Zhang, J. Z. *J. Phys. Chem. C* **2008**, *112*, 10323.
(40) Salt, I.; Gültekin, S. *React. Kinet. Catal. Lett.* **2004**, *83*, 253.
(41) Kumar, A.; Vemula, P. K.; Ajayan, P. M.; John, G. *Nat. Mater.* **2008**, *7*, 236.
(42) Jia, F.; Yu, C.; Deng, K.; Zhang, L. *J. Phys. Chem. C* **2007**, *111*, 8424.
(43) Yeh, F. H.; Tai, C. C.; Huang, J. F.; Sun, I. W. *J. Phys. Chem. B* **2006**, *110*, 5215.
(44) Sprunger, P. T.; Laegsgaard, E.; Besenbacher, F. *Phys. Rev. B* **1996**, *54*, 8163.

2 min, rinsed with ultra pure water, and dried with N_2. The alloy sample along with an aliquot of hfacH (Alfa Aesar, 99.9%) to achieve a concentration of 14 mM during processing were placed into a 50 mL high pressure batch reactor as previously described.[35] The reactor was charged with liquid CO_2 (99.99%), heated for 15 min to the supercritical processing conditions of 60 ± 5 °C and 16 ± 1 MPa (160 ± 10 bar), and then allowed to react for an additional 5 min. Etching was stopped by venting the CO_2. For simultaneous oxidation and dealloying, a AgCu sample was placed into the batch reactor with aliquots of both liquid H_2O_2 and hfacH to achieve equimolar concentrations of 14 mM during processing. The reactor was charged with liquid CO_2 (99.99%), heated for 15 min to the supercritical processing conditions of 60 ± 5 °C and 16 ± 1 MPa, and then allowed to react for an additional 20 min. H_2O_2 spontaneously decomposes into O_2 and H_2O and by reacting with Cu.[35,45] The maximum amount of O_2 that could be generated by the low oxidant concentrations examined in this study negligibly affected the reaction pressure, and inclusion of H_2O_2 in the $scCO_2$ solution did not pose other hazards. With both processes, chemicals contacted a AgCu sample only when the reactor was filled with liquid CO_2. The time that a sample was exposed to a supercritical fluid was used as a metric to compare sequential and simultaneous processes because it correlated with the amount of copper etched. This convolutes the detailed temporal variations in oxidant and chelator concentrations, temperature, and contacting phase, which undoubtedly differed between the two preparation methods.

The alloy surface morphology was characterized using a Hitachi S-4500 field-emission scanning electron microscope (FESEM) operating at 15 keV accelerating voltage. Stereo micrographs of the sample surface were captured and used to create a 3D anaglyph image (Alicona MeX software). Compositional FESEM images showing the microstructure of the as-received AgCu alloy were obtained from a sample mechanically polished to a 1 μm scratch using standard techniques. The compositions of the two phases were determined from energy-dispersive X-ray analysis with a Thermo Noran NSS detector. Sample surface species were analyzed using a Physical Electronics 549 X-ray photoelectron spectrometer with a double pass cylindrical mirror analyzer and a 400 W X-ray gun (Al Kα radiation). High resolution scans were taken at 50 eV pass energy and all spectra were aligned based on the adventitious C 1s peak at 284.6 eV. Spectra were fit with a least-squares method using a Shirley background and Gaussian line shapes for the purpose of deconvoluting into individual states and obtaining peak areas. X-ray diffraction (XRD) was performed on a Scintag XDS 2000 with CuKα radiation at 40 kV accelerating voltage and 40 mA. UV−vis data were collected using a Jasco V-670 spectrometer equipped with an integrating sphere. A planar 200 nm Ag film was deposited on to a clean Si substrate by electron beam evaporation (Edwards, Auto 306) for optical comparison to npAg.

Results and Discussion

Reacting a preoxidized AgCu alloy sample with hfacH in $scCO_2$ formed randomly shaped ligaments and pores as shown by the FESEM images in Figure 2. A control sample oxidized in liquid H_2O_2 and exposed to pure CO_2 had a nearly featureless surface (Figure 2a). After undergoing one cycle of the oxidation/etching process, evenly sized ~20 nm clusters appeared (Figure 2b). Following two etching cycles, these clusters increased in diameter and noticeable voids began to form (Figure 2c). The onset of full scale dealloying was observed after four oxidation/etching cycles (Figure 2d). Darker areas correspond to material removal and the taller, brighter regions show the more noble Ag metal atoms that conglomerated. The ligament size is on the order of 50−100 nm. An anaglyph image highlighting the three-dimensional structure of the dealloyed surface is shown in Figure S1 of the Supporting Information. Because the oxidation process is self-limiting, the stepwise images in Figure 2a−d represent a time profile of the nanoporous structure formation. The pattern of small clusters sequentially growing to larger ligaments closely resembles simulated models for liquid phase dealloying.[24] This suggests that despite differing methods of selective dissolution, the physical mechanisms responsible for pore formation in liquid and $scCO_2$ processes may be similar.

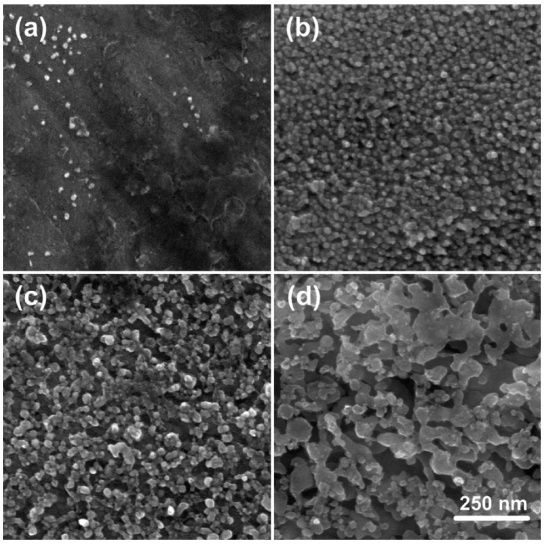

Figure 2. FESEM images of a AgCu alloy after (a) H_2O_2 oxidation and pure $scCO_2$ exposure, (b) 1 cycle of sequential oxidation/etching, (c) 2 cycles of oxidation/etching, and (d) 4 cycles of oxidation/etching. The scale bar is 250 nm and applies to all four images.

Corresponding XPS spectra of the progressively dealloyed AgCu surface are given in Figure 3. Gaussian fits of the Cu 2p binding energy region (Figure 3a) show that prior to etching, there were two states of Cu on the surface.The spin−orbit split peaks at 952.5 eV ($2p_{1/2}$) and 932.3 eV ($2p_{3/2}$) are attributed to Cu(0) metal and $Cu(I)_2O$. Differentiation between these oxidation states is not possible based on the 2p peaks alone because the binding energy separation is only 0.1 eV.[46] Fully oxidized Cu(II)O is also present, as indicated by both a second set of spin−orbit split peaks shifted by 1.3 ± 0.2 eV to higher binding energy and the appearance of characteristic satellite peaks at 962 and 942 eV. This CuO on the surface before intentional oxidation in H_2O_2 came from exposure to atmospheric oxygen over time. Liquid-phase H_2O_2

(45) Campestrini, S.; Tonellato, U. *Adv. Synth. Catal.* **2001**, *343*, 819.

(46) Moulder, J. F.; Stickle, W. F.; Sobol, P. E.; Bomben, K. D. *Handbook of X-ray Photoelectron Spectroscopy*; Physical Electronics, Inc.: Eden Prairie, MN, 1995.

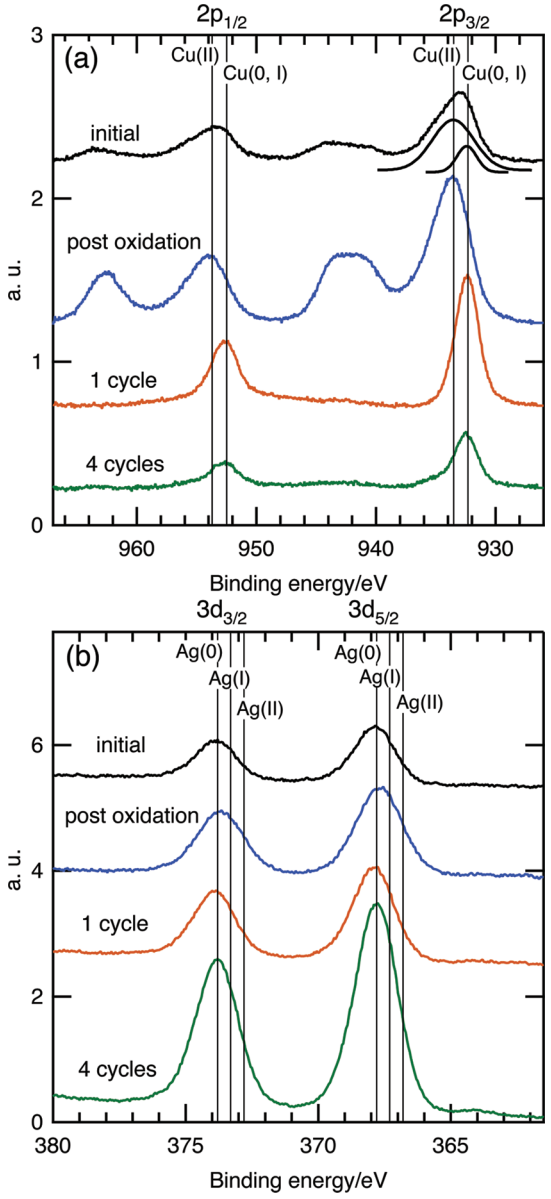

Figure 3. XPS spectra of a AgCu sample initially, after oxidation, after 1 sequential oxidation/etching cycle, and after 4 cycles in the (a) Cu 2p and (b) Ag 3d binding energy ranges.

oxidation of the alloy fully converted the copper on the surface to CuO as shown by the post oxidation XPS spectrum. After one reaction cycle with the hfacH/$scCO_2$ mixture, the satellite peaks disappeared and the Cu 2p peaks shifted to slightly lower binding energy, indicating CuO was completely removed. Following four oxidation and etching cycles, the XPS spectrum showed no residual CuO and a lower peak intensity, signifying a decrease in the relative amount of Cu in the surface region probed by XPS.

Figure 3b contains analogous XPS spectra for the Ag 3d states. The spin−orbit split Ag peaks at 373.8 eV ($3d_{3/2}$) and 367.8 eV ($3d_{5/2}$) are assigned to Ag metal. Although silver is a noble metal, it can exist in a 1+ or 2+ oxidation state with expected anomalous shifts to lower binding energies by 0.3 and 0.7 eV, respectively.[47] The fixed Ag 3d peak positions throughout the stepwise dealloying process indicate the liquid phase H_2O_2 process was aggressive enough to oxidize the Cu species, but left the Ag atoms in a metal state. After four processing cycles, the relative amount of Ag on the alloy surface increased. This was expected because there was a relative decrease in the surface concentration of Cu. Comparison of XPS peak areas to the known starting AgCu composition yields an estimated change in surface composition from 40 to 6 at % Cu after four stepwise dealloying cycles. The Cu signal is due to photoelectrons from exposed regions of the bulk alloy that are incompletely attenuated by the porous Ag overlayer. Analysis of the three-dimensional nanostructure from the anaglyph image (see Figure S1 in the Supporting Information) yields an approximate average feature height of 180 ± 80 nm following four etching cycles at a peroxide concentration that is about one-seventh of the solubility limit. This feature height is a reasonable estimate for the alloy etch depth as long as the overall porosity remains close to the starting Cu volume percentage of 33%.

A 5 min/cycle etching time was chosen for sequential dealloying because it was the minimum reaction time that yielded complete removal of CuO to the detection limit of XPS. Although hfacH is not expected to react with the surface once the oxide layer has been etched, longer cycle reaction times of 10 and 20 min were tested. These prolonged samples showed no superficial CuO and exhibited comparable FESEM surface morphology to those etched for 5 min. Self-limiting liquid phase H_2O_2 oxidation of pure Cu metal is reported to generate a 50 nm CuO layer.[37,48] Assuming oxidation of the AgCu alloy behaved similarly and formed a 50 nm thick oxide film yields a nominal dealloying rate of 10 nm/min. This value is ten times higher than that measured for oxidized blanket Cu films under similar conditions.[37] The higher etching rate for the AgCu alloy based on depth is reasonable because there were proportionately fewer copper atoms in a given volume compared to a pure blanket Cu film. However, the depth of copper oxidation could have been less than 50 nm for the alloy samples because of protection by metallically bonded silver atoms.[38] Also, CuO etching could have occurred in the 15 min heating period to reach supercritical conditions. The comparable rates for CuO etching from bulk Cu and the AgCu alloy indicates that the diffusion of Ag atoms on the surface is fast and does not limit the reaction rate.

The FESEM and XPS data in Figures 2 and 3 illustrates that Cu was selectively etched from a AgCu alloy leaving behind a porous network enriched in Ag. Further analysis using XRD (see Figure S2 in the Supporting Information) confirmed that the dealloying process generated a surface composed primarily of pure crystalline Ag and that the initial starting sample contained both a Ag-rich and a Cu-rich phase. In liquid solutions, multiphase metals can dealloy if one or more of the phases meet the conditions

(47) Weaver, J. F.; Hoflund, G. B. *J. Phys. Chem.* **1994**, *98*, 8519.

(48) Nishizawa, H.; Tateyama, Y.; Saitoh, T. *Thin Solid Films* **2004**, *455*, 491.

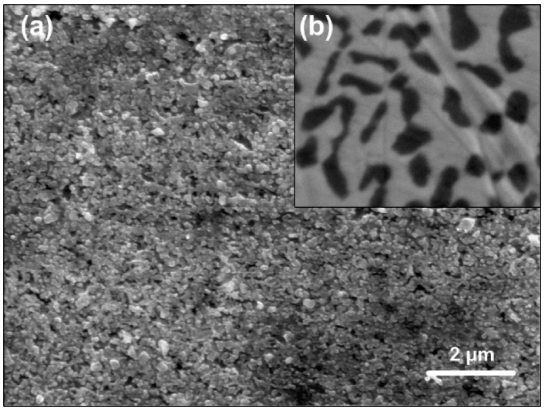

Figure 4. (a) Low-magnification FESEM image of a sequentially dealloyed AgCu surface and (b) compositional image showing the dark Cu-rich and lighter Ag-rich phases in the starting AgCu alloy. The scale bar is 2 μm and applies to both images.

necessary for selective dissolution.[30] Figure 4 shows a low-magnification FESEM image of a selectively etched layer in comparison to a compositional image (inset) of the specific eutectic AgCu alloy used in this study. Acquiring a compositional SEM image requires removing morphological contrast through polishing; consequently, a compositional image of a dealloyed surface cannot be obtained. The alloy initially contained dark, ~1 μm Cu-rich (77.8 at% Cu) lamella dispersed in a lighter Ag-rich phase (24.2 at% Cu). After etching in $scCO_2$, there were no structural features visible that correlated with the micrometer length scale in the phase map. Both phases were selectively etched, but formed similar morphologies that were indistinguishable based on SEM. These results are consistent with fast Ag atom surface diffusion.

One restriction for liquid phase dealloying is the parting limit, defined as the less noble metal concentration below which selective etching will not occur. It is interesting that dealloying was observed in the Ag-rich phase containing only 24.2 at % Cu because parting limits are often much higher for systems like AgCu with a relatively small $\Delta\phi$.[25] For example, AuAg will not dealloy below 60 at % Ag.[26] Dealloying in a low Cu content phase could be a unique property of the AgCu system or a result of the purely chemical supercritical dealloying process employed. Measured parting limits higher than the metal percolation threshold have been attributed to the electrolyte being unable to penetrate the small pores formed at low concentrations of the more reactive metal.[26] Fluid access is not a limitation during supercritical dealloying where low surface tension and viscosity allow the etching solution to wet and penetrate any size feature.

While cycling through separate oxidation and etching steps is useful for monitoring the progression of dealloying, it is more functional to combine the two steps by adding an oxidant to the $scCO_2$/hfacH mixture. This simultaneous processing approach allows for continuous Cu removal and should only be limited by depletion of the etching agents, most likely through decomposition of H_2O_2. Figure 5a and b show FESEM images of a sample before and after dealloying with an in situ oxidant.

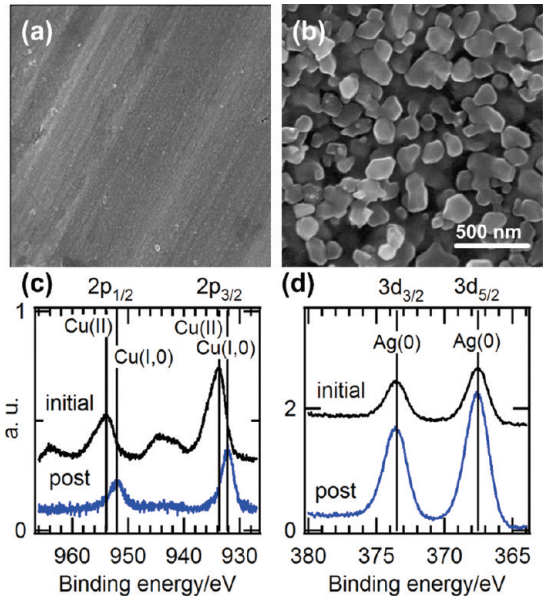

Figure 5. FESEM images of a AgCu alloy (a) initially and (b) after simultaneous oxidation and dealloying, and XPS spectra of the (c) Cu 2p and (d) Ag 3d binding energy ranges. The scale bar is 500 nm and applies to both images.

Uniform, 100−200 nm faceted, particle-shaped features formed on the surface after exposure to the $scCO_2$ etching solution. Although dealloyed surfaces often exhibit a network of ligaments like Figure 2d, structures similar to Figure 5b have also been reported.[28] XPS spectra in the Cu 2p and Ag 3d binding regions (Figure 5c and d) confirm that selective etching of Cu occurred leaving a Ag-rich surface. Based on the XPS peak areas, the surface concentration dropped from 39.9 to 9.5 at % Cu after the simultaneous dealloying process. The difference in size-scale and morphology between the sequentially and simultaneously oxidized and dealloyed samples is notable, especially considering XPS analysis showed that both processing methods produced similar surface compositions. It may be that the continuous time spent in $scCO_2$ solution allowed for increased surface conglomeration of the Ag atoms producing larger, more symmetric features during in situ dealloying. Most important, it emphasizes that the oxidation step plays an integral role in determining surface structure for dealloying in $scCO_2$ and could be used to control the nanoporous metal properties.

Differences in the two morphologies formed by dealloying with sequential and simultaneous oxidation were evident by their optical behavior. Ag nanostructures can interact with light and exhibit localized surface plasmon resonance (LSPR). The size, shape, and orientation of the nanostructures control how the conduction electrons resonate on a Ag surface under incident light and ultimately, the functionality of the material.[49,50] For example, tuning the mean grain size between 25 and 110 nm in a solution-deposited Ag film generated a 30% increase in the surface-enhanced Raman spectroscopy (SERS)

(49) Kreibig, U.; Vollmer, M. *Optical Properties of Metal Clusters*; Springer-Verlag: Berlin, Germany, 1995.
(50) Kelly, K. L.; Coronado, E.; Zhao, L. L.; Schatz, G. C. *J. Phys. Chem. B* **2003**, *107*, 668.

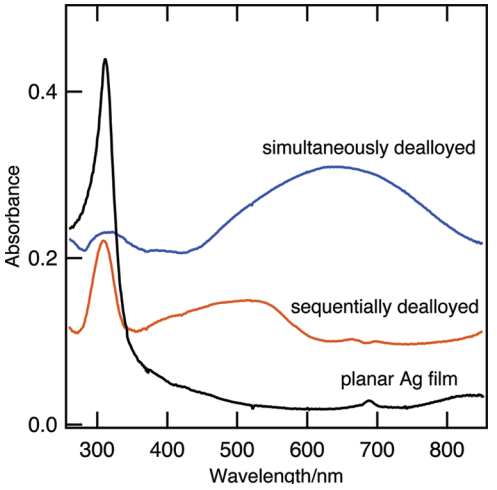

Figure 6. UV−vis absorbance spectra of npAg from sequentially and simultaneously dealloyed AgCu samples compared to an evaporated, planar Ag film.

enhancement factor to a value of $\sim 2 \times 10^5$ for absorbed benzenethiol.[51] The characteristic localized surface plasmon modes on a metal surface can be readily identified using UV−vis spectroscopy.

Figure 6 shows UV−vis absorbance spectra from both sequentially and simultaneously oxidized and dealloyed npAg surfaces in comparison to a nonstructured evaporated Ag film. The peak appearing at 317 nm in all three spectra corresponds to the bulk plasma edge of silver, which atypically appears in the near UV due to the unique position of the Ag d-orbitals with respect to the Fermi energy.[52] Dealloying produced two features at visible wavelengths. The Ag ligaments in the sequentially dealloyed sample exhibited an asymmetric absorbance centered in the green range (500−570 nm), which is consistent with published reports of LSPR on nanostructured Ag surfaces with characteristic length scales in the 50−100 nm regime.[51,53] The asymmetry of the peak results from the convolution of resonances along the major and minor axes of the elongated ligaments.[50] Comparatively, the LSPR absorbance for the simultaneously dealloyed sample consisting of larger 100−200 nm features is shifted to a peak value at ~650 nm in the red range. According to classical Mie theory, which is generally valid for particles larger than ~10 nm, LSPR peaks shift to longer wavelengths with increasing particle radius.[49] The more uniform size and evenly shaped particles on the in situ oxidized surface resulted in a symmetric LSPR absorption. This demonstrates that the optical properties produced by a specific surface morphology of npAg can be tuned using the processing conditions.

(51) Park, H. K.; Yoon, J. K.; Kim, K. *Langmuir* **2006**, *22*, 1626.
(52) Wooten, F. *Optical Properties of Solids*; Academic Press, Inc.: New York, 1972.
(53) Schmid, G.; Levering, M.; Sawitowski, T. *Z. Anorg. Allg. Chem.* **2007**, *633*, 2147.

Conclusion

Nanoporous Ag was formed by dealloying AgCu in $scCO_2$. The dealloying process proceeds by selective oxidation and subsequent dissolution of CuO. As Cu is preferentially etched, the Ag atoms conglomerate into superficial nanostructures with morphologies that depend on the processing method and that have distinct optical properties. The npAg length scale is an important parameter for determining not only optical behavior, but chemical and mechanical properties as well. Typical surface areas of nanoporous metals with ligament sizes of ~100 nm are on the order of 1 m^2/g, and the smaller features observed in the sequentially etched samples would yield a higher area, more ideal for devices such as chemical sensors.[4] Finite control over feature size would allow tuning of the material properties for a specific application. Although a 10 nm/min dealloying rate is relatively low to produce macroscopic structures, these results demonstrate a pathway for the large-scale and low environmental impact formation of nanoporous metals. The expected etching products are $Cu(hfac)_2$, H_2O, unreacted hfacH, and potentially $Ag(hfac)_2$. These could be collected and separated from CO_2 after processing by dropping the solution pressure. Reuse of the chemicals would depend on the application and could require additional separation and purification steps. Future work aims to better understand the underlying mechanisms for selective etching in high-pressure $scCO_2$ and thereby gain additional control over the properties of the nanoporous material.

Acknowledgment. R.M. gratefully acknowledges support from the American Association of University Women (AAUW) Selected Professions Fellowship, the Achievement Rewards for College Scientists (ARCS) Foundation, and the University of Arizona Chapman Fellowship. We are grateful to Kristina Dorame for experimental assistance and to Philip Anderson (Department of Material Science and Engineering, University of Arizona) for the XRD data.

Supporting Information Available: Additional FESEM characterization of the npAg and XRD spectra of the alloy before and after processing are given in the Supporting Information. This material is available free of charge via the Internet at http://pubs.acs.org/.